

# Direct transformation of graphene to fullerene

Andrey Chuvilin<sup>1,2\*</sup>, Ute Kaiser<sup>1</sup>, Elena Bichoutskaia<sup>3</sup>, Nicholas A. Besley<sup>3</sup> and Andrei N. Khlobystov<sup>3\*</sup>

**Although fullerenes can be efficiently generated from graphite in high yield, the route to the formation of these symmetrical and aesthetically pleasing carbon cages from a flat graphene sheet remains a mystery. The most widely accepted mechanisms postulate that the graphene structure dissociates to very small clusters of carbon atoms such as C<sub>2</sub>, which subsequently coalesce to form fullerene cages through a series of intermediates. In this Article, aberration-corrected transmission electron microscopy directly visualizes, in real time, a process of fullerene formation from a graphene sheet. Quantum chemical modelling explains four critical steps in a top-down mechanism of fullerene formation: (i) loss of carbon atoms at the edge of graphene, leading to (ii) the formation of pentagons, which (iii) triggers the curving of graphene into a bowl-shaped structure and which (iv) subsequently zips up its open edges to form a closed fullerene structure.**

Over the past two decades, many different models have been proposed to explain the formation of fullerene from graphite. The generally accepted mechanisms can be categorized into four major groups according to the exact route leading to the fullerenes: the 'pentagon road'<sup>1–3</sup>, the 'fullerene road'<sup>4</sup>, 'ring coalescence'<sup>5,6</sup> and the 'shrinking hot giant model'<sup>7,8</sup>. All of these can be classified as bottom-up mechanisms, because fullerene cages are considered to be formed from atomic carbon or small clusters of carbon atoms. Although there is a large body of experimental evidence supporting bottom-up mechanisms<sup>9–11</sup>, it is almost entirely based on mass spectrometry and its variants, which analyse only those species present in the gas phase. These experiments provide no direct structural information about the precursors of fullerenes and do not allow fullerene formation to be followed *in situ*. Any process of fullerene assembly on the surface of graphite, for example, would be overlooked by the traditional experimental methodology.

An atomically thin single sheet of graphite, so-called graphene<sup>12</sup>, represents an ideal viewing platform for molecular structures using transmission electron microscopy (TEM), because it provides a robust and low-contrast support for molecules and other nanoscale species adsorbed on the surface. Under TEM observation while exposed to an 80-keV electron beam (e-beam), the edges of the graphene sheet appear to be continuously changing in shape (Fig. 1a; see also Supplementary Video). The high energy of the e-beam, when transferred to the carbon atoms of the graphene, can cause fragmentation of large sheets of graphene into smaller flake-like structures (Fig. 1c). The flakes adsorbed on the graphene substrate can be visualized and their further transformations readily observed in TEM. The final product of these transformations is often a perfect fullerene molecule (Fig. 1b).

The sequence shown in Fig. 1c–h presents a typical transformation route for an individual graphene flake, which changes its shape under the influence of the e-beam, becoming increasingly round (Fig. 1c–e). The contrast of its edges gradually increases (Fig. 1f), indicating that the edges of the flake come progressively out of plane and rearrange into the spheroidal shape of a fullerene (Fig. 1g). The experimentally observed images can be related through TEM image simulation to models of a graphene flake (Fig. 2b'), curved graphene intermediates (Fig. 2d' and e'), and

the resultant fullerene molecule (Fig. 2f') adsorbed on the graphene substrate. Once fullerene formation is complete, the molecule appears to roll back and forth on the underlying graphene (Fig. 1h). This is possible, because the energy of the van der Waals interaction of a fullerene with the substrate is significantly reduced compared to a flat graphene flake<sup>13,14</sup> due to the reduced surface area in contact with the underlying graphene sheet.

Loss of carbon atoms at the edge of graphene is a key initial step in the graphene-to-fullerene transformation. Carbon atoms at the edge of a graphene flake are labile, because only two bonds connect them to the rest of the structure. Our density functional theory (DFT) calculations (for details see the Methods section) show that the loss of a carbon atom at the zigzag edge of a small graphene flake and the subsequent relaxation of the structure require 5.4 eV. As expected, it is approximately one-third less than the energy of carbon atom loss from the middle of the flake, which is estimated to be 7.4–7.6 eV (refs 15–17). Indeed, recent TEM experiments have demonstrated that the edge atoms of graphene can be chipped away, one by one, by the e-beam<sup>18,19</sup>. Following the removal of one or several carbon atoms, the graphene edge undergoes structural reconstruction, normally leading to the most stable zigzag configuration<sup>18</sup>. The loss of carbon atoms at the edge and the subsequent reconstruction do not cause any significant changes to the structure of a large graphene sheet<sup>18,19</sup> (Supplementary Fig. S1). However, small fragments of graphene, as our extended observations demonstrate (Supplementary Fig. S2), undergo drastic structural transformations under the e-beam, leading to the formation of fullerene cages (Fig. 1c–h). These observations provide direct evidence (unlike mass spectrometry) that a fullerene can be formed directly from graphene without the need for dissociation to small carbon clusters as is inherent to other mechanisms of fullerene formation<sup>1,2,20</sup>.

The experimental TEM images provide compelling evidence for the graphene-to-fullerene transformation. However, the exact pathway of this process can be best explained through quantum chemical modelling of the key stages of the process (Fig. 2a–f). The structures used for modelling represent one possible flake that is as close as possible to the experimental observations (Fig. 1c–h). Induced by the high-energy e-beam, the initial loss of carbon atoms at the edge destabilizes the structure (Fig. 2b),

<sup>1</sup>University of Ulm, Central Facility of Electron Microscopy, Electron Microscopy Group of Materials Science, Albert Einstein Allee 11, 89069 Ulm, Germany,

<sup>2</sup>IKERBASQUE, Basque Foundation for Science, E-48011, Bilbao, Spain, <sup>3</sup>School of Chemistry, University of Nottingham, University Park, Nottingham

NG7 2RD, UK. \*e-mail: a.chuvilin@nanogune.eu; andrei.khlobystov@nottingham.ac.uk

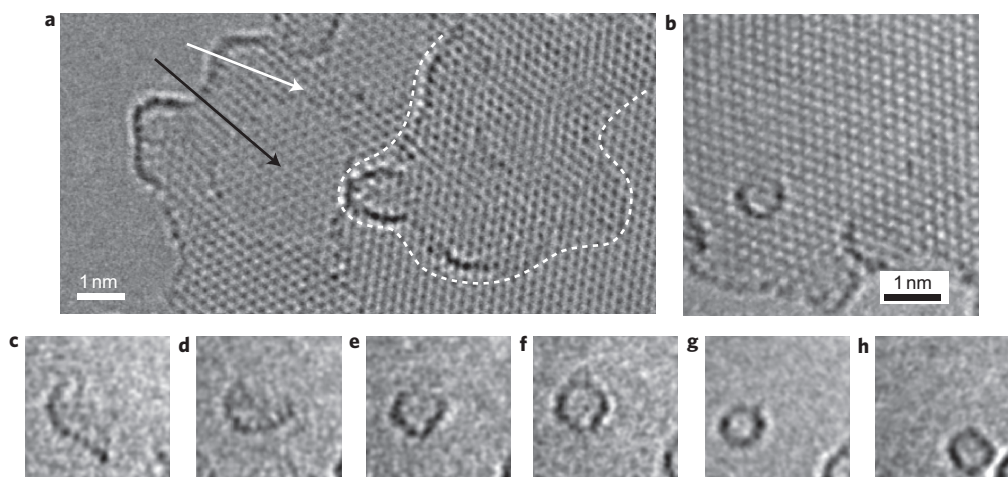


**Figure 1 | Experimental TEM images showing stages of fullerene formation directly from graphene.** **a**, The black arrow indicates a double layer of graphene, which serves as the substrate. The white arrow indicates a strip of graphene (monolayer) adsorbed on this substrate. The dashed white line outlines a more extended island of graphene mono- or bi-layer, which has its edges slightly curved on the left side. **b**, The final product of graphene wrapping: a fullerene molecule on the surface of graphene monolayer (carbon atoms appear as black dots). **c–h**, Consecutive steps showing the gradual transformation of a small graphene flake (**c**) into fullerene (**g,h**). The graphene lattice is filtered out of images **c–h** for clarity. (See Supplementary Video for a demonstration of the dynamics of the entire process.)

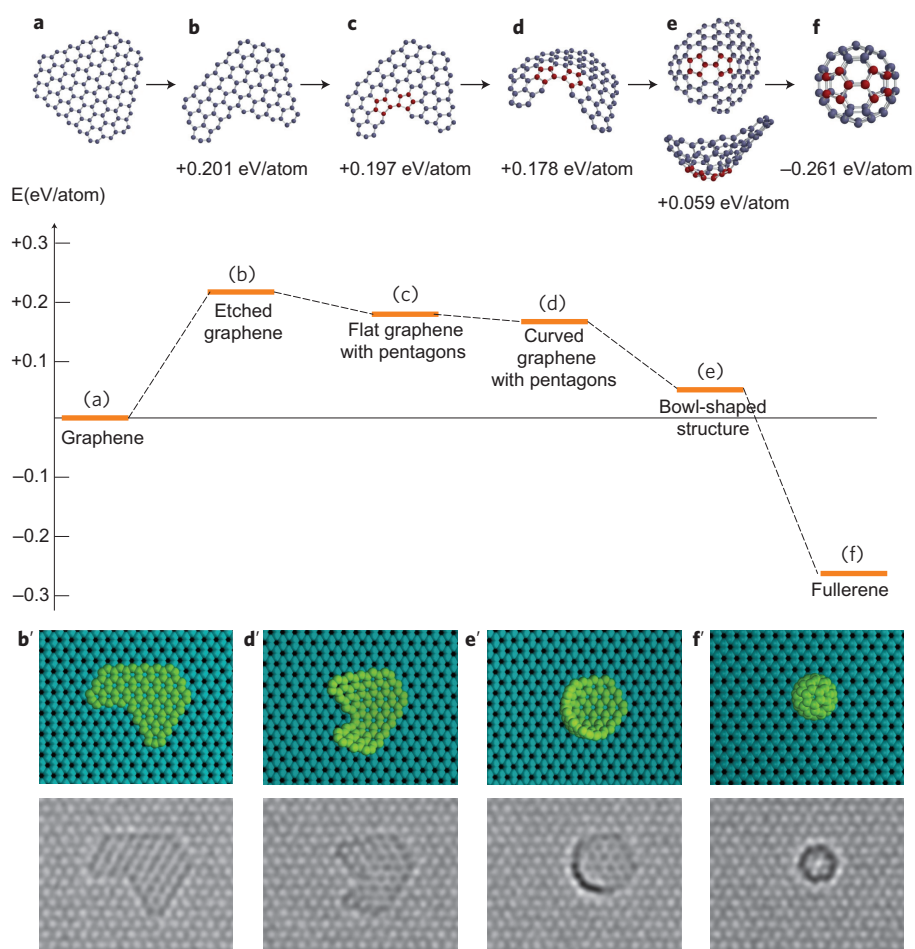


**Figure 2 | Quantum chemical modelling of the four critical stages of fullerene formation from a small graphene flake.** **a–d**, Loss of carbon atoms at the edge (**a** → **b**); formation of pentagons (**b** → **c**); curving of the flake (**c** → **d**); formation of new bonds, leading to zipping of the flake edges (**d** → **e**). **e**, Top and side views of a bowl-shaped intermediate structure. Stabilization energies (in eV per carbon atom) of the intermediate structures and resultant fullerene  $C_{60}$  (**f**), relative to the flat defect-free flake of graphene shown in **a**, are presented pictorially and graphically. **b',d'–f'**, Top views of the graphene flake (**b'**), curved graphene intermediates (**d',e'**) and the fullerene  $C_{60}$  molecule (**f'**) adsorbed on the underlying graphene substrate and simulated TEM images corresponding to each structure, showing how they would appear in TEM experiments.

because it increases the number of dangling bonds at the edge. The formation of pentagons at the edge (Fig. 2c) and subsequent curving of the flake are thermodynamically favourable processes, because they bring covalently deficient carbon atoms close to one another (Fig. 2d), thus enabling them to form bonds. New carbon–carbon bonds are then formed, leading to zipping of the flake edges and reducing the number of dangling bonds. This has a profound stabilizing effect on the structure (Fig. 2e). In a similar way, the bowl-shaped structure (Fig. 2e) can evolve further by losing carbon atoms from its remaining open edge through e-beam etching, forming more pentagons and curling until the structure is sufficiently small to close up into a cage (Fig. 2f). Fullerene is the most stable configuration for a finite number of  $sp^2$  carbon atoms because the molecular cage has no open edges (that is, etching is prohibited), and all the carbon atoms form three bonds. If the structure of the newly formed fullerene does not correspond to the most stable isomer, its structure can ‘anneal’ by means of a series of Stone–Wales rearrangements<sup>1</sup> that are facilitated by the e-beam in TEM or by an add-atom under the standard fullerene synthesis conditions<sup>21,22</sup>.

A theoretical study exploring the possibility of the transformation of a graphene sheet into a fullerene confirms that the formation of defects at the edge of graphene is the crucial step in the process<sup>20</sup>. The structural defects considered in this earlier study are based on a series of rearrangements that give rise to pentagonal rings. However, the energy barrier for such rearrangements appeared to be extremely high, making this pathway plausible only at extremely high temperatures (3,500 K)<sup>20</sup>, significantly higher than the temperatures used in fullerene production. Our calculations, however, show that the loss of the outermost carbon atoms in a graphene flake provides a viable route for fullerene formation under realistic experimental conditions.

The initial size of the graphene flake is important, because it determines the size of the fullerene cage that can be formed. If the flake is too large, in the region of several hundreds of carbon atoms, there will be a significant energetic penalty during the curving step (Fig. 2d) associated with the van der Waals interactions between the underlying graphene sheet and the flake. Its edges will continue to be etched until the flake reaches a size that enables the thermodynamically driven formation of fullerene described above. On the other hand, the transformation of very small flakes (less than 60 carbon atoms) into fullerenes will be suppressed by excessive strain on C–C bonds imposed by the high curvature of small fullerene cages and the violation of the isolated pentagon rule in fullerenes smaller than  $C_{60}$ . Indeed, our experiments indicate that fullerene cages formed directly from graphene have a relatively narrow range of diameters averaging  $\sim 1$  nm, which corresponds to 60–100 carbon atoms (Supplementary Fig. S2). This observation is in agreement with the consistent observation of a disproportionately high abundance of  $C_{60}$  and  $C_{70}$  fullerenes found in the different methods of fullerene production.

Our *in situ* TEM experiments correlated with quantum chemical modelling demonstrate that a direct transformation of flat graphene sheets to fullerene cages is possible. Etching of edge carbon atoms by the e-beam facilitates the formation of curved graphene fragments, which continue to be etched until it becomes possible for them to zip up into a fullerene. Previous studies have suggested that a piece of graphene of limited size may not be the most stable allotrope of carbon<sup>23–25</sup>, particularly under e-beam radiation, so the latter stages of this thermodynamically driven process should occur with similar ease to the formation of  $C_{60}$  fullerene from carefully designed polyaromatic molecules<sup>26</sup>. Once the edges are sealed, no further carbon atoms can be lost, and the newly created fullerene remains intact under the e-beam.

Could these TEM observations be relevant to real-life fullerene production methods, such as arc discharge or laser ablation of

graphite? On the one hand, conditions inside the transmission electron microscope are quite different (for example, no direct heating, high vacuum, no buffer gas), but on the other hand, the e-beam supplies the energy required to break chemical bonds (just like a laser beam), and the underlying graphite substrate attached to a TEM sample holder absorbs the excess energy released on the formation of new bonds (just like a helium buffer-gas). Indeed, a mass spectrometry study<sup>27</sup> has shown that  $C_{60}$  and  $C_{70}$  can form almost exclusively from graphite under 10-keV e-beam radiation in vacuum—conditions very similar to those in TEM—but no mechanism explaining fullerene formation was suggested at the time. The top-down mechanism of fullerene formation proposed in our study does not exclude the bottom-up models, because different mechanisms may co-exist under the same experimental conditions (Supplementary Fig. S3). For example, in arc discharge, some fullerenes may form in the gas phase from  $C_2$  fragments and some may form on the surface of graphite electrodes from small flakes of graphene. A laser ablation study<sup>28</sup> has shown that the yield of fullerene is critically dependent on the orientation and quality of the graphitic surface, which confirms that the formation of fullerene directly on the graphite surface is certainly not unique for TEM experiments and may have relevance for preparative methods of fullerene production. We hope that our study will stimulate a reassessment of the current understanding of how fullerenes are formed.

## Methods

Thin graphite flakes were prepared from spectroscopically pure graphite by grinding in an agate mortar under a layer of ethanol. The dispersion was treated as prepared in an ultrasonic bath and deposited onto a holey carbon TEM grid. Stacks of graphene with thicknesses varying between one and several layers were observed.

Images were acquired using a Titan 80-300 instrument (FEI) equipped with an imaging spherical aberration (Cs) corrector. We used an accelerating voltage of 80 kV and Cs optimized Scherzer conditions<sup>29</sup> (Cs value,  $+20 \mu\text{m}$ ; defocus,  $-3 \text{ nm}$ ), so the atoms were imaged dark. The exposure time was 1 s per frame, with an interval of 4 s between the frames in one sequence (Supplementary Video). Images of one sequence were aligned by cross-correlation and low-pass-filtered for noise reduction. The filtering did not affect the final resolution because of significant over-sampling of the original images.

TEM image simulations were performed using MUSLI code<sup>30</sup>. Coherent aberrations corresponding to those in the experimental images were used. Parameters for the dumping envelope were as follows: focal distance, 1.5 mm (tabulated value for Titan 80-300); coefficient of chromatic aberration, 1.4 mm (measured experimentally); energy spread of the electron source, 0.2 eV (measured experimentally); stability of high tension,  $1 \times 10^{-6}$  (tabulated value for Titan 80-300); stability of objective lens current,  $3 \times 10^{-7}$  (fitted by simulations); convergence semi-angle, 0.5 mrad (this parameter does not measurably influence aberration-corrected imaging). Thermal vibrations were treated using the frozen phonons approach, with 100 phonon configurations averaged for every image at a corresponding Debye–Waller factor of 0.005  $\text{nm}^2$ . The sampling rate was 0.017  $\text{nm pixel}^{-1}$ . Images were calculated at an electron dose of  $1 \times 10^6 \text{ e}^- \text{ nm}^{-2}$  and further processed using the same routine as for the experimental images (see above).

In theoretical calculations of the geometries and energies of the intermediates, the description of a small graphene flake, which initially contained 117 carbon atoms and was subsequently reduced to 86 and 84 atoms, was based on the DFT formalism using the Q-CHEM quantum chemistry package<sup>31</sup> with the B3LYP exchange–correlation functional<sup>32</sup> and 6-31G\* basis set.

Dispersive van der Waals interactions between the graphene flake and the underlying graphene sheet contribute up to  $\sim 30\%$  reduction in its stabilization energy, depending on the size and curvature of the fragment. The energy of these non-covalent interactions was estimated using the empirical Girifalco potential, which has been successfully applied to describe the interactions between graphitic nanostructures<sup>13</sup>.

Received 5 November 2009; accepted 19 March 2010;  
published online 9 May 2010

## References

1. Smalley, R. E. Self-assembly of the fullerenes. *Acc. Chem. Res.* **25**, 98–105 (1992).
2. Goroff, N. S. Mechanism of fullerene formation. *Acc. Chem. Res.* **29**, 77–83 (1996).
3. Kroto, H. W. & McKay, K. The formation of quasi-icosahedral spiral shell carbon particles. *Nature* **331**, 328–331 (1988).



4. Heath, J. R. Synthesis of  $C_{60}$  from small carbon clusters: a model based on experiment and theory. *ACS Symp. Ser.* **481**, 1–23 (1991).
5. Hunter, J. M., Fye, J. F., Roskamp, E. J. & Jarrold, M. F. Annealing carbon cluster ions—a mechanism for fullerene synthesis. *J. Phys. Chem.* **98**, 1810–1818 (1992).
6. Rubin, Y., Kahr, M., Knobler, C. B., Diederich, F. & Wilkins, C. L. The higher oxides of carbon  $C_{8n}O_{2n}$  ( $n=3-5$ ): synthesis, characterization and X-ray crystal structure. Formation of cyclo[n]carbon ions  $C_n^+$  ( $n=18, 24$ ),  $C_n^-$  ( $n=18, 24, 30$ ), and higher carbon ions including  $C_{60}^+$  in laser desorption Fourier transform mass spectrometric experiments. *J. Am. Chem. Soc.* **113**, 495–500 (1991).
7. Irle, S., Zheng, G., Wang, Z. & Morokuma, K. The  $C_{60}$  formation puzzle ‘solved’: QM/MD simulations reveal the shrinking hot giant road of the dynamic fullerene self-assembly mechanism. *J. Chem. Phys. B* **110**, 14531–14545 (2006).
8. Huang, J. Y., Ding, F., Jiao, K. & Yakobson, B. I. Real time microscopy, kinetics and mechanism of giant fullerene evaporation. *Phys. Rev. Lett.* **99**, 175503 (2007).
9. Yannoni, C. S., Bernier, P. P., Bethune, D. S., Meijer, G. & Salem, J. R. NMR determination of the bond lengths in  $C_{60}$ . *J. Am. Chem. Soc.* **113**, 3190–3192 (1991).
10. Hawkins, J. M., Meyer, A., Loren, S. & Nunlist, R. Statistical incorporation of carbon-13  $^{13}C_2$  units into  $C_{60}$  (buckminsterfullerene). *J. Am. Chem. Soc.* **113**, 9394–9395 (1991).
11. Ebbesen, T. W., Tabuchi, J. & Tanigaki, K. The mechanistics of fullerene formation. *Chem. Phys. Lett.* **191**, 336–338 (1992).
12. Geim, A. K. & Novoselov, K. S. The rise of graphene. *Nature Mater.* **6**, 183–191 (2007).
13. Girifalco, L. A. & Hodak, M. Van der Waals binding energies in graphitic structures. *Phys. Rev. B* **65**, 125404 (2002).
14. Ulbricht, H., Moos, G. & Hertel, T. Interaction of  $C_{60}$  with carbon nanotubes and graphite. *Phys. Rev. Lett.* **90**, 095501 (2003).
15. El-Barbary, A. A., Telling, R. H., Ewels, C. P., Heggie, M. I. & Briddon, P. R. Structure and energetics of the vacancy in graphite. *Phys. Rev. B* **68**, 144107 (2003).
16. Saito, M., Yamashita, K. & Oda, T. Magic numbers of graphene multivacancies. *Jpn J. Appl. Phys.* **46**, L1185–L1187 (2007).
17. Carlsson, J. M. & Scheffler, M. Structural, electronic and chemical properties of nanoporous carbon. *Phys. Rev. Lett.* **96**, 046806 (2006).
18. Girit, C. O. *et al.* Graphene at the edge: stability and dynamics. *Science* **323**, 1705–1708 (2009).
19. Jia, X. *et al.* Controlled formation of sharp zigzag and armchair edges in graphitic nanoribbons. *Science* **323**, 1701–1705 (2009).
20. Lozovik, Y. E. & Popov, A. M. Formation and growth of carbon nanostructures: fullerenes, nanoparticles, nanotubes and cones. *Uspekhi Fizicheskikh Nauk* **167**, 751–774 (1997).
21. Eggen, B. R. *et al.* Autocatalysis during fullerene growth. *Science* **272**, 87–90 (1996).
22. Ioffe, I. N. *et al.* Fusing pentagons in a fullerene cage by chlorination: IPR  $D_2C_{76}$  rearranges into non-IPR  $C_{76}Cl_{24}$ . *Angew. Chem. Int. Ed.* **48**, 5904–5907 (2009).
23. Ugarte, D. Curling and closure of graphitic networks under electron-beam irradiation. *Nature* **359**, 707–709 (1992).
24. Burden, A. P. & Hutchison, J. L. An investigation of the electron irradiation of graphite in a helium atmosphere using a modified electron microscope. *Carbon* **35**, 567–578 (1997).
25. Füller, T. & Banhart, F. *In situ* observation of the formation and stability of single fullerene molecules under electron irradiation. *Chem. Phys. Lett.* **254**, 372–378 (1996).
26. Otero, G. *et al.* Fullerenes from aromatic precursors by surface-catalysed cyclodehydrogenation. *Nature* **454**, 865–868 (2008).
27. Bunshah, R. F. *et al.* Fullerene formation in sputtering and electron beam evaporation processes. *J. Phys. Chem.* **96**, 6866–6869 (1992).
28. Xie, Z.-X. *et al.* Formation and coalescence of fullerene ions from direct laser vaporization. *J. Chem. Soc. Faraday Trans.* **91**, 987–990 (1995).
29. Scherzer, O. The theoretical resolution limit of the electron microscope. *J. Appl. Phys.* **20**, 20–29 (1949).
30. Chuvin, A. & Kaiser, U. On the peculiarities of CBED pattern formation revealed by multislice simulation. *Ultramicroscopy* **104**, 73–82 (2005).
31. Shao, Y. *et al.* Advances in methods and algorithms in a modern quantum chemistry program package. *Phys. Chem. Chem. Phys.* **8**, 3172–3191 (2006).
32. Becke, A. D. A new mixing of Hartree–Fock and local density-functional theories. *J. Chem. Phys.* **98**, 1372–1377 (1993).

### Acknowledgements

This work was supported by the Engineering and Physical Sciences Research Council (Career Acceleration Fellowship to E.B., grant no. EP/C545273/1 to A.N.K.), the European Science Foundation, the Royal Society, the DFG (German Research Foundation) and the State Baden-Württemberg within the SALVE (Sub Angström Low Voltage Electron Microscopy) project and by the DFG within Collaborative Research Centre (SFB) 569.

### Author contributions

A.C. conceived, designed and carried out experiments. U.K. contributed to the development of the experimental methodology and the discussion of the results. E.B. and N.A.B. performed theoretical modelling and contributed equally to this work. A.N.K. proposed the mechanism and wrote the original manuscript. All authors discussed the results and commented on the manuscript.

### Additional information

The authors declare no competing financial interests. Supplementary information accompanies this paper at [www.nature.com/naturechemistry](http://www.nature.com/naturechemistry). Reprints and permission information is available online at <http://npg.nature.com/reprintsandpermissions/>. Correspondence and requests for materials should be addressed to A.C. and A.N.K.